Pointing calibration campaign at 21 GHz with K-band multi-feed receiver

R.Verma, L.Gregorini, I.Prandoni, A.Orfei

IRA 441/11

February 17, 2011

Contents

List of Tables

Abstract

We present an analysis of 9 bright radio sources (3C48, 3C84, 3C147, 3C273, 3C286, 3C295, 1611+343, DR21 and NGC7027) observed at 21 GHz with the new 7-horn K-band multi-feed receiver (MF) coupled with the total power analog backend. These sources were mostly selected from the calibrator list of Baars et al.(1977). The main objective of this report is to check the pointing of the receiver and to quantify the pointing offsets. In addition we are aimed at building a calibrator list for the Medicina 32-m telescope to be used for 21 GHz MF observations and in particular for the planned 21 GHz survey of the northern sky with MF. We will also report on three calibrators (3C48, 3C147 and 3C286) observed during the 21 GHz pilot survey, carried out at Medicina with the same system. An area of 1000 square degrees covering the North celestial polar cap ranging from declination 72° to 90° was mapped using On The Fly mapping technique. These three calibrators were used to check the pointing of MF and to calibrate the data. In this report we will present results on the pointing of the MF receiver.

Conventions and Abbreviations

The conventional abbreviations for Systéme international d'unités (SI) units and astronomical quantities are used. The following abbreviations have been used in this report:

- Count - The radio signal in an arbitrary backend unit.
- Dec - Declination.
- Delta Dec - Difference between the actual declination of the source (taken from the literature (commanded)) and the one obtained after the gaussian fitting to the scans.
- Delta RA - Difference between the actual right ascension of the source (taken from the literature (commanded)) and the one obtained after the gaussian fitting to the scans in right ascension.
- deg - Degree, unit of the angle
- dn - Number of measurements in each bin.
- El - Elevation.
- FWHM - Full width at half maximum.
- FWHM (Dec) - Full width at half maximum of antenna beam in declination direction.
- FWHM (RA) - Full width at half maximum of antenna beam in right ascension direction.
- LCP - Left circular polarization.
- RA - Right ascension.
- RCP - Right circular polarization.

1 Pointing Model

Using a pointing model is a routine practice among radio-telescopes devoted to astronomy. The basic model used at most radio telescope is a variant of the model described by Ulich (1981) (parallel work on pointing models for optical telescope, Wallace, 1975). The general philosophy at the heart of these models is that the model should reflect the real effects, such as axis misalignments, flexures etc. These imperfections as well as gravity or any remaining systematic errors should be removed using empirical functions. Recent developments in pointing algorithms advocates the use of empirical functions such as spherical harmonics, to describe the pointing model.

1.1 Primary pointing equations

In the following we describe the physical model for telescope pointing. The azimuth and elevation terms used to correct the nominal source positions ($A_{command}$ and $E_{command}$ respectively) are given by the equations:

$$\begin{aligned} \Delta A &= IA + CA\sec(E) + NPAE\tan(E) + AN\tan(E)\sin(A) \\ &\quad - AW\tan(E)\cos(A) + A_{obs}\sec(E) \end{aligned} \tag{1}$$

$$\Delta E = IE + ECEC\cos(E) + AN\cos(A) + AW\sin(A) + E_{obs} + R(P_s, T_s, RH, E) \tag{2}$$

where A and E are the azimuth and elevation of the source and the individual pointing coefficient are listed in Table1. Therefore the azimuth and elevation of the target sources is given by:

$$A_{encoder} = A_{command} + \Delta A \tag{3}$$

$$E_{encoder} = E_{command} + \Delta E \tag{4}$$

where ΔA & ΔE are the total azimuth and elevation encoder correction.

1.2 Secondary pointing equations

The secondary pointing equations are also necessary together with the primary pointing equations to correct for the off-axis placement of receivers. These correction equation can be given by:

$$\Delta A_1 = IA_1 + CA_1\sec(E) \tag{5}$$

$$\Delta E_1 = IE_1 + ECEC_1\cos(E) \tag{6}$$

where ΔA_1 corresponds to the 'cross-elevation'azimuth correction on the sky, given at a particular elevation by the observer-applied azimuth correction. IA_1 & CA_1 are the supplemental

Table 1: Basic telescope pointing model terms. ; col.(1) gives the notation of the term.; col.(2) gives the physical meaning of the term.

Term[a]	Physical Meaning
IA	Azimuth encoder offset
CA	Collimation error of the electromagnetic axis
NPAE	Non-perpendicularity between the mount azimuth and elevation axes
AN	Azimuth axis offset/misalignment north-south
AW	Azimuth axis offset/misalignment east-west
A_{obs}	Observer-applied azimuth correction
IE	Elevation encoder offset
ECEC	Gravitational flexure correction at the horizon
E_{obs}	Observer-applied elevation correction
R(P_s,T_s,RH,E)	Atmospheric refraction correction, which is a function of ambient pressure (P_s), temperature T_s, relative humidity (RH) and the elevation of the source

[a]We use the notation developed in the TPOINT pointing analysis program.

azimuth encoder offset & supplemental electromagnetic collimation error correction respectively, while IE_1 & $ECEC_1$ are the supplemental elevation encoder offset and supplemental gravitational bending error respectively.

1.3 Additional terms

There are other additional physical deformations of the telescope structure which can be introduce in the pointing model. They are listed as:

(1) For radio telescopes with a wheel-and-track azimuth mount, it is often necessary to correct for the irregularities in the azimuth tracks as a function of azimuth.

(2) If elevation drive /encode is miscentered it leads to an additional gravity flexure, a term sin(E) should also be included in the pointing model for the overall gravity correction.

1.4 Determining coefficients & rms pointing error

The coefficients mentioned in Eq. 4, 5, 8 and 9 are derived from the collection of the 50 or more pointing measurements. These measurements should be performed in such a way to represent the telescope pointing behavior over all the azimuth and elevation to allow a linear least-square fit to

Eq. 4 & 5. The terms A_{obs} and E_{obs} are observer-applied corrections based on individual pointing measurements made during an astronomical observation. Also each receiver in the bay has its own set of secondary coefficient to compensate for the feed and mirror alignment in case of off-axis placement.

Once these coefficients are obtained, a simultaneous linear least-square fit of the coefficients in Eq. 4 & 5 is carried out to minimize the mean-squared pointing error. Then these coefficients are inserted into the mount control software to be used to calculate the necessary pointing corrections. We should also mention that these coefficients are updated frequently to update the pointing model of the telescope.

1.5 Pointing model and expected rms pointing error for MF receiver at Medicina telescope

In previous section we have given a general philosophy of pointing model and listed all the terms in Table 1 which can be used in pointing algorithms but it is not necessary to use all of them. For the MF at Medicina telescope we use 8 pointing coefficients to describe the pointing model and the observer - applied azimuth and elevation correction (A_{obs} & E_{obs}) is not possible to be included in the current pointing model. Also the atmospheric refraction correction is performed after the retrieval of pointing model. As there are no off-axis receivers at Medicina telescope, secondary pointing equations are not used in pointing models. **The rms pointing error for MF receiver in both azimuth and elevation direction at Medicina telescope is approximately 6-8 arcsec in normal weather conditions**. The description of the pointing model currently in use is given as: pointing model number - 00011, model generation time - 17/Jan/2009.

2 Observing System

The Istituto di Radioastronomia (INAF, Bologna) is on the way to complete the commissioning of the K-band multi-feed receiver (MF), built for the upcoming 'Sardinia Radio Telescope (SRT)'. The MF is a 7-horn receiver arranged in a hexagonal geometry with a central feed. It spans a frequency band from 18 to 26 GHz with an instantaneous bandwidth of 2 GHz. The first phase of the commissioning of the MF started at the Medicina 32-m dish in 2008 while waiting for the SRT to be completed. Since the total power analog backend and the new antenna control system ESCS were both under development, we coupled them with the Medicina 32-m telescope to test the entire system. A calibration campaign was launched in September 2009 to check the pointing of the receiver. Eight bright radio sources were observed during this campaign. In winter 2010 a pilot survey was conducted as part of the commissioning of the MF to check the scientific performance

of the receiver. In the following sections we will firstly describe the pointing calibration campaign and then the pilot survey. We will mostly focus on the issues concerning the telescope pointing.

3 Pointing Calibration Campaign

Calibration procedures compensate for the imperfections and unknowns of an instrument including antenna defects, atmospheric transmission, receiver, backend gain and pointing errors etc. To obtain precise flux density of the source, antenna should be properly pointed at the source. Therefore telescope pointing plays an important role in astronomy. The standard radio flux density calibrators are the best candidates to check the pointing of the receiver and to derive the gain of the telescope.

3.1 Target Selection

We have selected 8 bright calibrators. Most of these sources belong to the calibrator list of Baars et al.(1977) except the sources 3C84, 3C273 and 1611+343. The selected sources have the following characteristics:

(1) flux density greater than 1.0 Jy at 21 GHz.

(2) angular size less than 100 arcsec, the FWHM of the Medicina antenna beam at 21 GHz.

(3) no intraday flux variation.

(4) a power law radio spectrum.

Table 2 reports the source positions and the flux densities (in Jy) at 21 GHz. In Table 2 we also include source 3C147, which was not selected for the 2009 calibration campaign, but was later observed during the pilot survey in winter 2010 (see section 3 for more details). The flux densities at 21 GHz are calculated using different methods. For sources from Baars et al. (1977) calibrator list flux densities are calculated using the spectra based on the absolute spectrum of Cas(A) (Baars et al. 1977) where flux density can be represented as a function of frequency given by:

$$logS[Jy] = a + b * log\nu[MHz] + c * log^2\nu[MHz] \quad (7)$$

where S & ν are the flux density and frequency; and a, b, c are the spectral coefficients applicable in a certain frequency range. The flux densities for each source at 21 GHz are calculated using the Ott et al (1994) spectral coefficients.

In case of DR21 spectral coefficient were not available from Ott et al. (1994) because of the less reliable measurements therefore we have used the spectral coefficients from Baars et al. (1977)

For sources that do not belong to the Baars et al. (1977) calibrator list flux densities at 21 GHz are obtained using a linear interpolation between 10 GHz and 23 GHz measurements (Peng et al., 2000).

Table 2: Flux density of the selected sources at 21 GHz. ; col.(1) gives the extensively known name of the source, mostly 3C (Third Cambridge Radio Catalogue) source name; col. (2) and col.(3) give the source position coordinates: right ascension and declination in equatorial coordinate system; col. (4) S_{21GHz} corresponds to the expected flux density at 21 GHz.

Source Name	RA (hhmmss.s)	Dec (ddmmss)	S_{21GHz}(Jy)
3C48[a]	01 37 41.3	+33 09 35	1.29
3C84[b]	03 19 48.1	+41 30 42	17.56
3C147[a]	05 42 36.1	+49 51 07	1.88
3C273[b]	12 29 06.7	+02 03 09	34.26
3C286[a]	13 31 08.3	+30 30 33	2.56
3C295[a]	14 11 20.6	+52 12 09	1.01
1611+343[b]	16 13 41.0	+34 12 48	4.32
DR21[c]	20 37 14.0	+42 29 46	19.17
NGC 7027[a]	21 07 01.7	+42 14 11	5.53

[a] Flux density is calculated using the spectral coefficient from Ott et al.(1994) measurements.

[b] Flux density is calculated using linear interpolation between 10 GHz and 23 GHz measurements (Peng et al., 2000).

[c] Flux density is calculated using the spectral coefficient from Baars et al.(1977) measurements.

3.2 Observations & data reduction

K-band observations were carried out using the Medicina 32-m dish on September 27^{th} & 28^{th}, 2009 in the frequency band 20-22 GHz (central frequency 21 GHz) exploiting the central feed of the new K-band multi-feed receiver[1]. Each source was measured using cross-scan observations, where the scan was first performed in right ascension and then in declination. Each source was observed at different elevations through multiple cross scans. In total 178 cross-scans were performed and the data acquired through the total power analog backend with a sample rate of 40 ms. Since the receiver and the backend, together with the new antenna control system (Enhanced Single-dish Control System, ESCS) were undergoing commissioning, we have performed the cross-scans moving the antenna at different speeds, in order to check whether the antenna speed can induce different offsets in the antenna position parameters (both in right ascension and declination). In particular we have exploited two different antenna speeds: 3°/minute and 1.5°/minute. The data reduction consisted of three main steps: scan quality check, baseline subtraction and source fitting.

[1]For more details on the K-band multi-feed receiver refer to Verma et al. 2009, Internal Report IRA-430/09

As a result of quality check 12% of the RA scans and 17% of Dec scans were discarded due to the adverse effect of poor weather. Then a 1^{st} order polynomial was used for baseline subtraction of the remaining scans, and a six parameter non-linear least square fit, involving a Gaussian and a 2^{nd} order polynomial background was performed. The function fitted after the baseline removal is -

$$f(x) = A_0 \exp(-\frac{z^2}{2}) + B_1 + B_2 x + B_3 x^2 \tag{8}$$

&

$$z = \frac{x - A_1}{A_2} \tag{9}$$

Where A_0 is the amplitude of the Gaussian peak, A_1 is the position at which the peak of the Gaussian fit occurs, A_2 represents the width of the Gaussian (standard deviation, σ). B_1, B_2 and B_3 represent the constant, linear and quadratic terms of the 2^{nd} order polynomial respectively.

Figure 1 illustrates the reduction procedure for a scan performed in RA direction. In the top diagram we have the raw data showing a prominent non-flat baseline. In the bottom diagram we have the result of the Gaussian fitting performed with a 2^{nd} order polynomial background, after baseline subtraction.

3.3 Antenna parameters & pointing accuracy

In this section we discuss the pointing of the multi-feed receiver. In order to check the pointing of the receiver in both right ascension and declination direction, RA and Dec scans were analysed separately. The fitting function given in Eq.8 was applied to each RA and Dec scan. We retrieve the measured source positions (RA and Dec) and the FWHM of the antenna beam from the Gaussian fit. The expected FWHM of antenna beam is $\approx$ 100 arcsec at 21 GHz. The distribution the measured values of the FWHM of the antenna beam in both RA and Dec direction for all the observed sources is shown in Figures 2 & 3. In Figures 4 & 5 we also present the distribution of the differences between the source RA and Dec values used to point the telescope (taken from literature, see Table 2) and the ones measured through the source Gaussian fits.

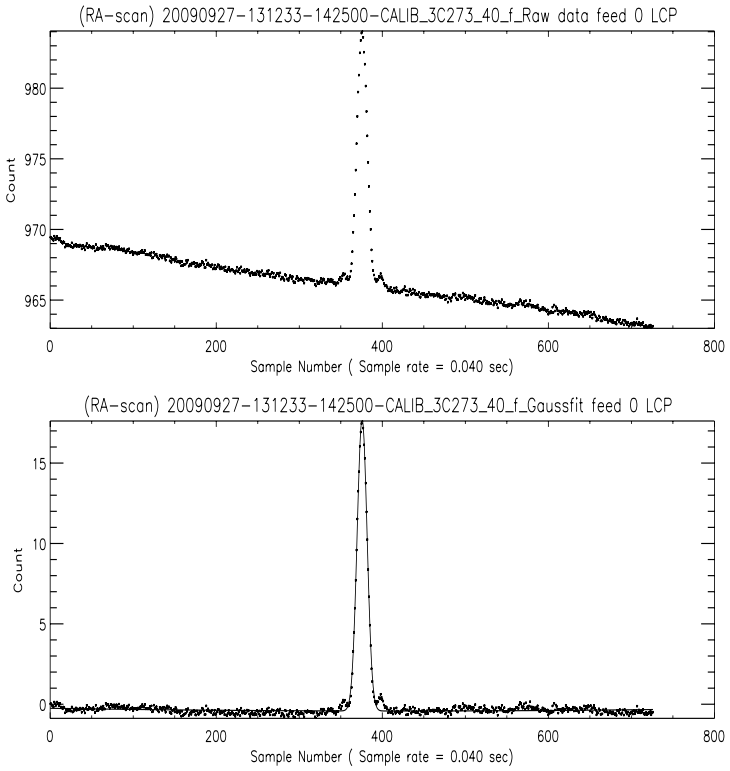

Figure 1: Scan across source 3C273 at an elevation of 40° with the central feed for left circular polarization. Top: Raw data, Bottom: Gaussian fit with a 2^{nd} order polynomial background, after baseline subtraction. X-axis represents the sample number (sample rate is 40 ms); Y-axis represents the signal in an arbitrary unit referred as Count.

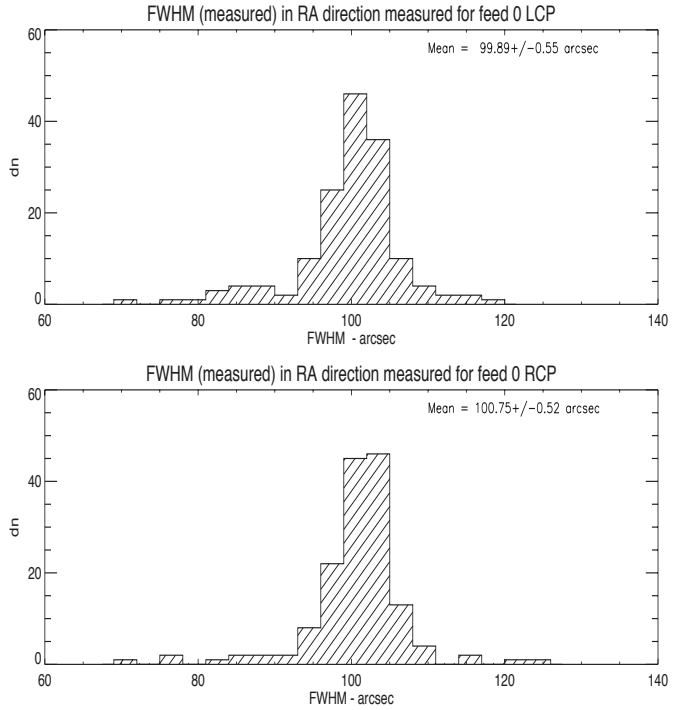

Figure 2: Histogram of the FWHM of the telescope beam (expected ≈ 100 arcsec) measured from the Gaussian fit in right ascension direction. Top: Left circular polarization; Bottom: Right circular polarization.

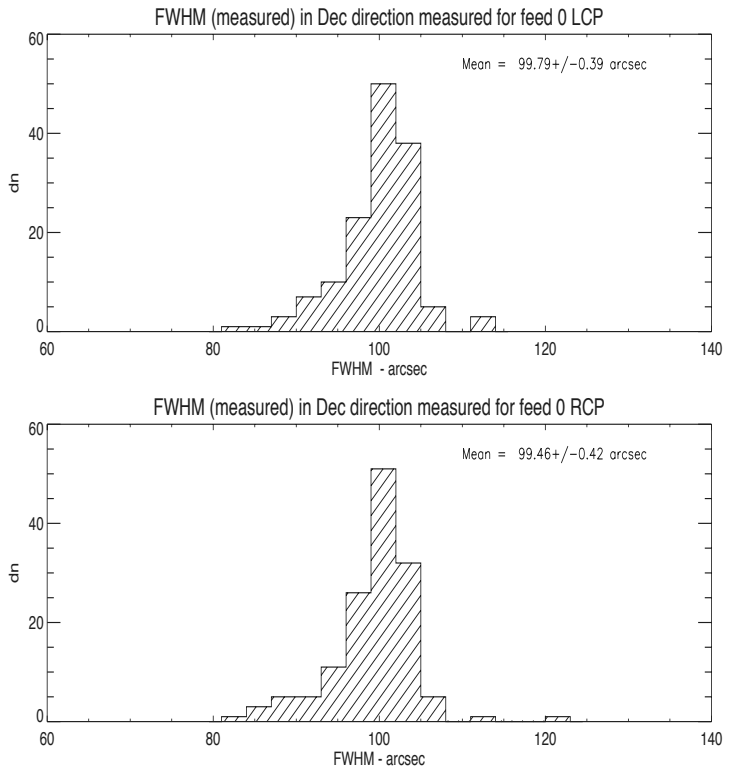

Figure 3: Histogram of the FWHM of the telescope beam (expected $\approx$ 100 arcsec) measured from the Gaussian fit in declination direction. Top: Left circular polarization; Bottom: Right circular polarization.

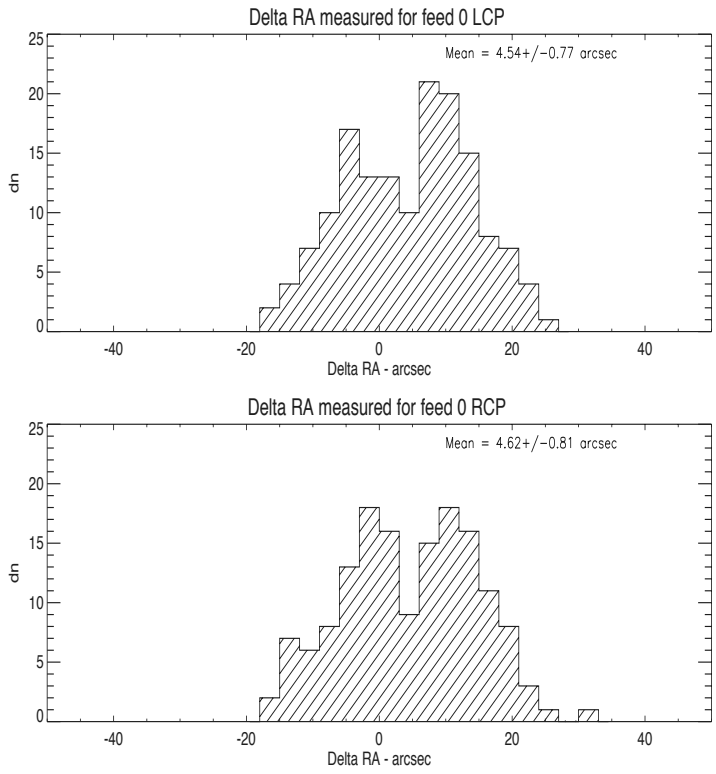

Figure 4: Histogram of the difference between the RA taken from the literature and the ones measured from the Gaussian fit in units of arcsec. Top: Left circular polarization; Bottom: Right circular polarization.

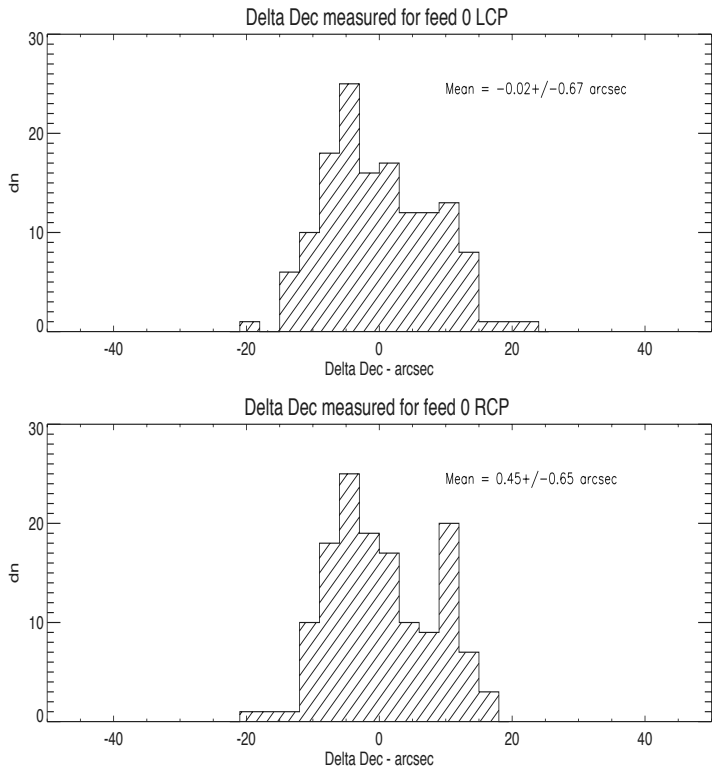

Figure 5: Histogram of the difference between the Dec taken from the literature and the ones measured from the Gaussian fit in units of arcsec. Top: Left circular polarization; Bottom: Right circular polarization.

All the aforementioned parameters measured through Gaussian fits are summarized in Table 3. A mean value FWHM of the antenna beam and the difference between the commanded and the measured values of RA and Dec is listed for each parameter.

Table 3: Antenna position parameters obtained through Gaussian fitting; col.(1) gives the name of the antenna parameter; col.(2) & col.(3) give the parameter value for the left circular polarization and right circular polarization.

Parameter	Feed 0 LCP Mean value (arcsec)	Feed 0 RCP Mean value (arcsec)
FWHM (RA)	99.89±0.55	100.75±0.52
FWHM (Dec)	99.79±0.39	99.46±0.42
Delta RA	4.54±0.77	4.62±0.81
Delta Dec	-0.02±0.67	0.45±0.65

As we have mentioned earlier, cross-scans were performed driving the antenna with two different speeds, 3.0°/minute & 1.5°/minute. In order to see any possible correlation between antenna speed and pointing accuracy of the telescope we have repeated the analysis after dividing RA scans into two groups: one with scans performed with an antenna speed of 3.0°/minute and the second one with antenna speed of 1.5°/minute. The number of scans performed with 1.5°/minute and 3.0°/minute of antenna speed in right ascension direction are 77 and 75 respectively. Similarly Dec scans were also divided into two groups. The number of scans performed with 1.5°/minute and 3.0°/minute of antenna speed in declination direction are 73 and 68 respectively.

The results are plotted in Appendix A and summarized in Table 4. We do not find any significant trend with antenna speed. The difference in parameter values at 1.5°/minute and 3°/minute are consistent within the error, with the only exception of Delta Dec for LCP where 3°/minute measurements show a larger offset.

Table 4: Antenna position parameters obtained through Gaussian fitting for the scans obtained with different antenna speeds; col.(1) gives the name of the antenna parameter.; col.(2) & col.(3) give the difference in parameter value for the left circular polarization for antenna speed of 1.5°/minute & 3.0°/minute respectively.; col.(4) & col.(5) give the difference in parameter value for the right circular polarization for antenna speed of 1.5°/minute & 3.0°/minute respectively.

Parameter	LCP mean (arcsec)		RCP mean (arcsec)	
	1.5°/minute	3.0°/minute	1.5°/minute	3.0°/minute
FWHM (RA)	99.89±0.88	99.90±0.64	100.49±0.81	101.03±0.66
FWHM (Dec)	99.26±0.57	100.36±0.52	99.11±0.53	99.84±0.66
Delta RA	3.09±1.02	6.19±1.14	3.53±1.11	5.81±1.15
Delta Dec	-0.47±0.91	5.84±0.52	-0.07±0.94	1.00±0.89

It is important to check whether pointing is stable for different sources. Measurements were therefore split for different elevations. The overall dependence of Delta RA and Delta Dec on

elevation averaging the scans of all the eight sources at each elevation is shown in Figures 6 and 7 respectively. We find that the pointing is stable for all elevations $\geq 40^{\circ}$. Low elevations $\leq 30^{\circ}$ show similar offsets but measurements seem to be uncorrelated to the ones obtained at higher elevations.

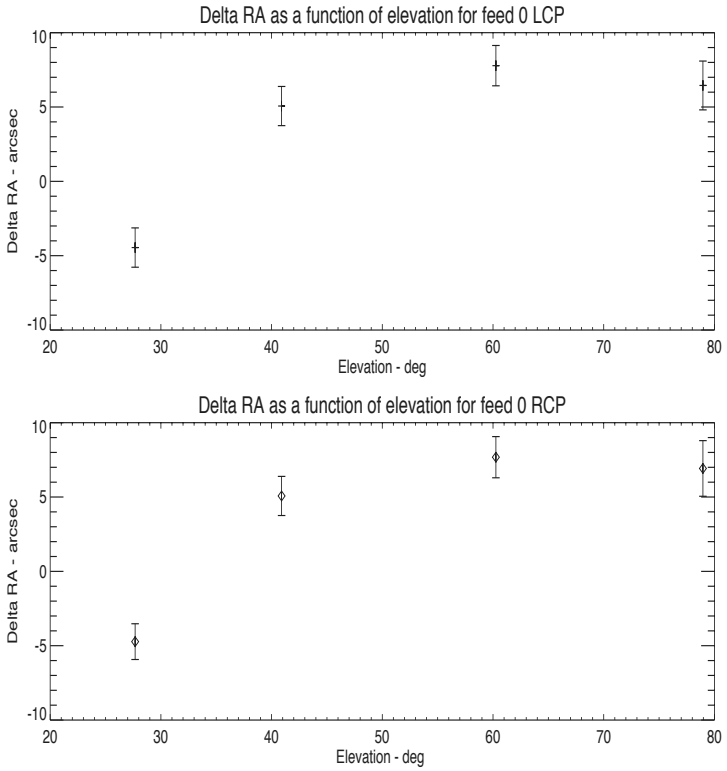

Figure 6: Delta RA (arcsec) versus elevation(degrees). Top: Left circular polarization; Bottom: Right circular polarization

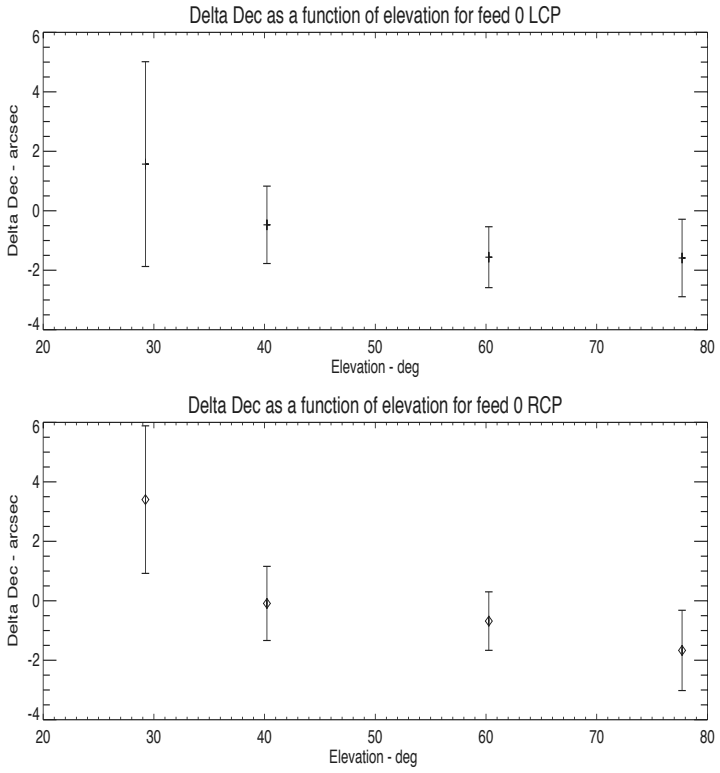

Figure 7: Delta Dec (arcsec) dependence on the elevation (degrees). Top: Left circular polarization; Bottom: Right circular polarization

Finally we have measured the FWHM of antenna beam and the offsets in RA & Dec for each source separately. Here we present the results for two sources, 3C48 and 3C286, as they are together with source 3C147 the calibrators used during the planned pilot survey at 21 GHz (see section 3). The total number of scans performed on source 3C48 and 3C286 are 16 and 58. 37% of 3C48 scans and 23% of 3C286 scans were discarded due to the adverse effect of weather. The results are plotted in Appendix B and listed in Table 5 (3C48) and Table 6 (3C286).

Table 5: Antenna position parameters obtained through Gaussian fitting to the source 3C48; col.(1) gives the name of the antenna parameter.; col.(2) & col.(3) give the parameter value for the left circular polarization and right circular polarization.

Parameter	Feed 0 LCP Mean value (arcsec)	Feed 0 RCP Mean value (arcsec)
FWHM (RA)	93.90±2.06	99.40±1.76
FWHM (Dec)	98.08±1.76	96.22±1.76
Delta RA	7.62±2.37	7.74±2.31
Delta Dec	0.79±1.18	3.32±2.16

Table 6: Antenna position parameters obtained through Gaussian fitting to the source 3C286; col.(1) gives the name of the antenna parameter.; col.(2) & col.(3) give the parameter value for the left circular polarization and right circular polarization.

Parameter	Feed 0 LCP Mean value (arcsec)	Feed 0 RCP Mean value (arcsec)
FWHM (RA)	101.33±1.64	102.56±1.25
FWHM (Dec)	97.65±1.61	97.48±1.19
Delta RA	6.95±1.54	5.64±1.55
Delta Dec	3.19±1.91	2.33±1.88

In conclusion, the pointing parameter accuracy is of the order of few arcsec independent of antenna speed and elevation for all the observed calibrators. It is also important to mention that both the sources 3C48 and 3C286 are among the weakest sources in Table2.

4 Pilot Survey

As mentioned earlier, a pilot survey was conducted in winter 2010 as part of the commissioning of the MF to check the scientific performance of the receiver. The survey was carried out to test the feasibility of an ambitious project: the K-band NOrthern Wide Survey (KNoWS) aimed at mapping the entire Northern sky. The pilot survey consisted in mapping an area of 1000 square degrees covering the North celestial polar cap at declination $> 72°$. The fully sampled mapping of the area was achieved in 4 days by performing azimuth scans between 0° - 25° with an antenna speed of 15°/minute at a constant elevation of 44.52° using On The Fly mapping technique[2] . In order to check the pointing and to perform flux calibration, three calibrators (3C48, 3C147 and 3C286) were observed approximately every six hours as they transit at the same elevation (45°). The positions and flux densities of these calibrators are given in Table 2 (see section 2).

[2]Refer to S.Righini PhD thesis, 2010

4.1 Antenna parameters & pointing accuracy

The sources were observed during the pilot survey from December 2009 to February 2010. Cross-scans were performed as for the calibration campaign, first in the right ascension and then in declination directions. In Table 7 we summarize the scan quality for each source.

Table 7: Observation summary for the sources observed during the pilot survey; col.(1) lists the source name.; col.(2) & col.(3) give the number of good quality RA and Dec scans.; col.(4) & col.(5) give the % of scans discarded due to poor weather.

Source	Good quality scans		% of discarded scans	
	RA scans	Dec scans	RA scans	Dec scans
3C48	36	36	30	30
3C147	22	18	40	50
3C286	60	60	23	23

The data reduction strategy to retrieve antenna parameters (Delta RA, Delta Dec and FWHM in both RA and Dec direction) is the same used for the calibration campaign (see section 2). The results obtained for each source are plotted in Appendix C and listed in Tables 8, 10 and 9 respectively. The offsets mean values measured during the pilot survey are in agreement with the ones measured during the calibration campaign for the same sources (see Tables 5 and 6) and with the overall offsets presented in Table 3.

Table 8: Antenna position parameters obtained through Gaussian fitting to the source 3C48; col.(1) gives the name of the antenna parameter.; col.(2) & col.(3) give the mean parameter offset for the left circular polarization and right circular polarization.

Parameter	Feed 0 LCP Mean value (arcsec)	Feed 0 RCP Mean value (arcsec)
FWHM (RA)	97.02±1.21	97.77±1.28
FWHM (Dec)	101.03±1.77	101.00±1.77
Delta RA	10.24±0.88	10.85±0.88
Delta Dec	-6.54±0.74	-6.11±1.03

Table 9: Antenna position parameters obtained through Gaussian fitting to the source 3C286; col.(1) gives the name of the antenna parameter.; col.(2) & col.(3) give the mean parameter offset for the left circular polarization and right circular polarization.

Parameter	Feed 0 LCP Mean value (arcsec)	Feed 0 RCP Mean value (arcsec)
FWHM (RA)	98.81±0.55	99.21±0.57
FWHM (Dec)	99.72±0.56	99.23±0.57
Delta RA	5.46±0.65	5.95±0.70
Delta Dec	-2.75±1.36	1.91±1.36

Table 10: Antenna position parameters obtained through Gaussian fitting to the source 3C147; col.(1) gives the name of the antenna parameter.; col.(2) & col.(3) give the mean parameter offset for the left circular polarization and right circular polarization.

Parameter	Feed 0 LCP Mean value (arcsec)	Feed 0 RCP Mean value (arcsec)
FWHM (RA)	99.36±1.03	101.08±1.15
FWHM (Dec)	98.97±1.00	101.54±1.15
Delta RA	-3.83±1.43	-4.82±1.28
Delta Dec	4.00±0.77	4.00±0.82

5 Conclusion

From the overall analysis presented here we can draw the following conclusions:

(1) The measured beam size at 21 GHz (100 arcsec) agrees with the expected value within offsets of the order of 1-4 arcsec in both right ascension and declination directions except in the case of the source 3C48 observed during calibration campaign offset in RA direction is approximately 6 arcsec.

(2) The measured RA and Dec positions can show very large offsets with respect to the ones used to point the telescope (up to 20-30 arcsec). However the mean offset values are typically of the order of 4-6 arcsec i.e. within the allowed telescope pointing precision ($\approx$ 1/10 of the antenna beam).

(3) There is no significant correlation between RA or Dec offsets and elevation, at least in the elevation range of 40° - 80°, where the mean values are of the same order of magnitude as the ones presented in Table 3. At very low elevations ($\leq$ 30°) the telescope pointing is less stable and different offsets are found.

(4) No significant correlation is found between antenna pointing parameters and antenna speed. The mean values of the offsets lie between 4-6 arcsec for any of the tested antenna speeds.

(5) The antenna parameters and pointing accuracy during the pilot survey are as good as the ones characterized in the calibration campaign.

Acknowledgements

R.Verma would like to thank Franco Mantovani for the arduous task of proof reading.
This research was supported by the EU Framework 6 Marie Curie Early Stage Training programme under contract number MEST-CT-2005-110069 '*ESTRELA*'.

References

[1] **Baars, J.W.M., et al.**,'The Absolute Spectrum of Cas A;
An Accurate Flux Density Scale and a Set of Secondary Calibrators', *1977, A&A , 61, 99.*

[2] **Mangum, J.G.**,'A Telescope Poiting Algorithm for ALMA', *ALMA Memo 366, 2001.*

[3] **Ott, M., et al.**,'An updated list of radio flux density calibrators', *1994, A&A, 284, 331O.*

[4] **Peng, B., et al.**,'Long-term monitoring of selected radio sources', *2000, A&AS, 145, 1P.*

[5] **Righini, S., PhD thesis**,'The Enhanced Single-dish Control System. and wide surveys of compact sources', *2010*, `http://urania.bo.astro.it/tesi/XXII/astrophysical_technologies/Righini_Simona.pdf`.

[6] **Ulich, B.L.**,'Millimeter wave radio telescopes: gain and pointing characteristics', *1981, International Journal of Infrared and Millimeter Waves, 2, 2.*

[7] **Verma, R., et al.**,'A new K-band (18-26 GHz) 7-horn multi-feed receiver: Calibration campaign at Medicina 32 m dish', 2009, *Internal Report, IRA 430/09.*

Appendix A

This appendix contains the diagrams showing offsets in RA, Dec and FWHM for the different antenna speeds. Data are taken from the calibration campaign carried out on 2009, September 27^{th} & 28^{th}.

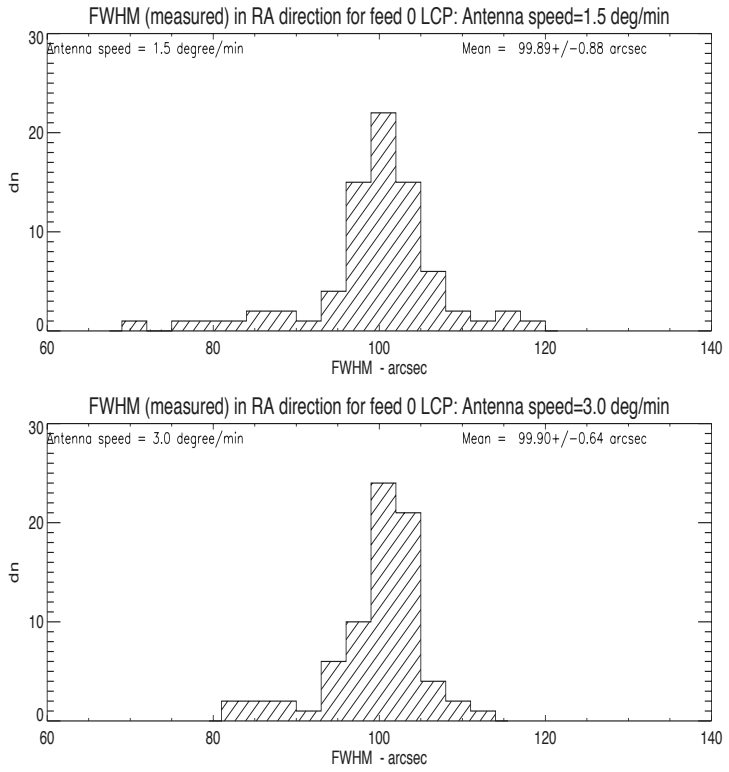

Figure 8: Histogram of the FWHM of the telescope beam (expected $\approx$ 100 arcsec) measured from the Gaussian fit in right ascension direction for left circular polarization. Top: Scans performed with antenna speed of 1.5°/minute; Bottom: Scans performed with antenna speed of 3.0°/minute.

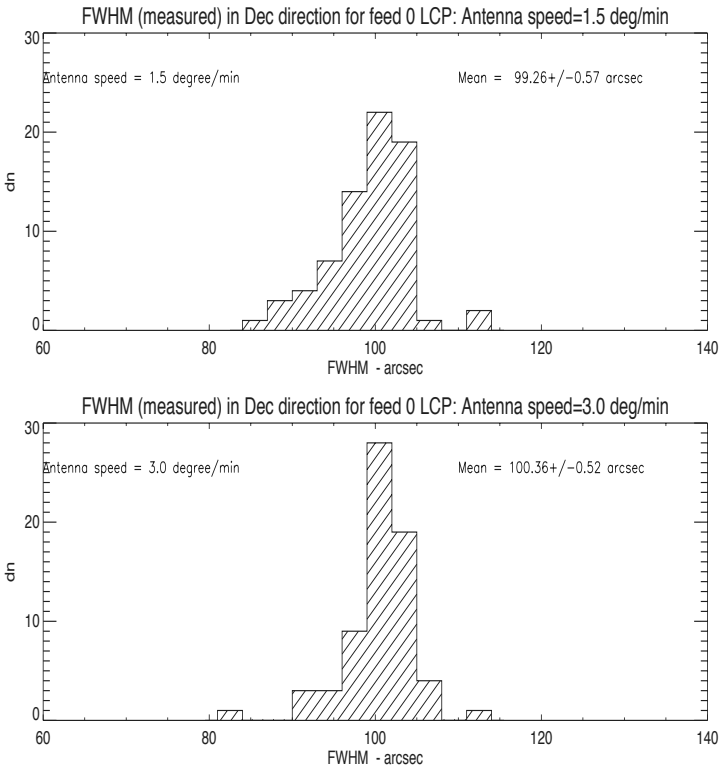

Figure 9: Histogram of the FWHM of the telescope beam (expected $\approx$ 100 arcsec) measured from the Gaussian fit in declination direction for left circular polarization. Top: Scans performed with antenna speed of 1.5°/minute; Bottom: Scans performed with antenna speed of 3.0°/minute

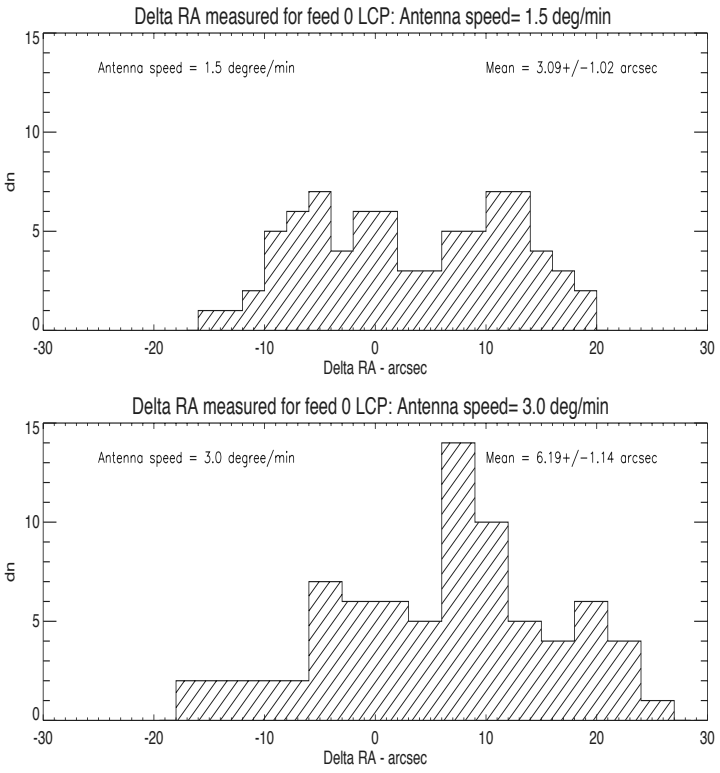

Figure 10: Histogram of the difference between RA taken from the literature and the ones measured from the Gaussian fit in units of arcsec for left circular polarization. Top: Scans performed with antenna speed of 1.5°/minute; Bottom: Scans performed with antenna speed of 3.0°/minute

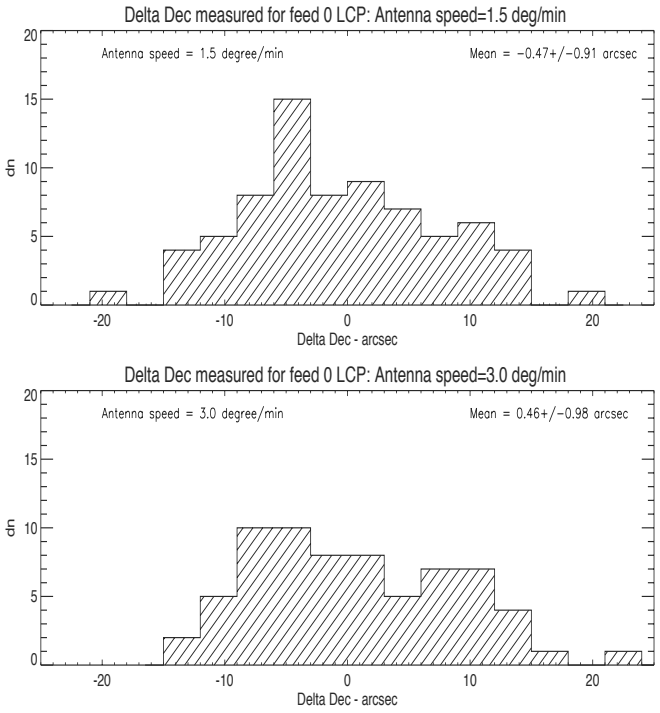

Figure 11: Histogram of the difference between Dec taken from the literature and the ones measured from the Gaussian fit in units of arcsec for left circular polarization. Top: Scans performed with antenna speed of 1.5°/minute; Bottom: Scans performed with antenna speed of 3.0°/minute

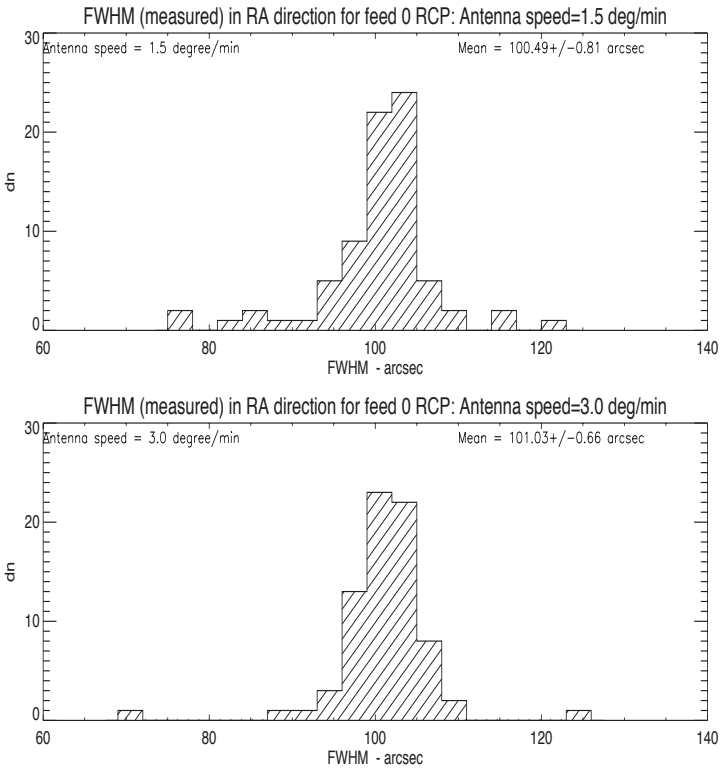

Figure 12: Histogram of the FWHM of the telescope beam (expected $\approx$ 100 arcsec) measured from the Gaussian fit in right ascension direction for right circular polarization. Top: Scans performed with antenna speed of 1.5°/minute; Bottom: Scans performed with antenna speed of 3.0°/minute.

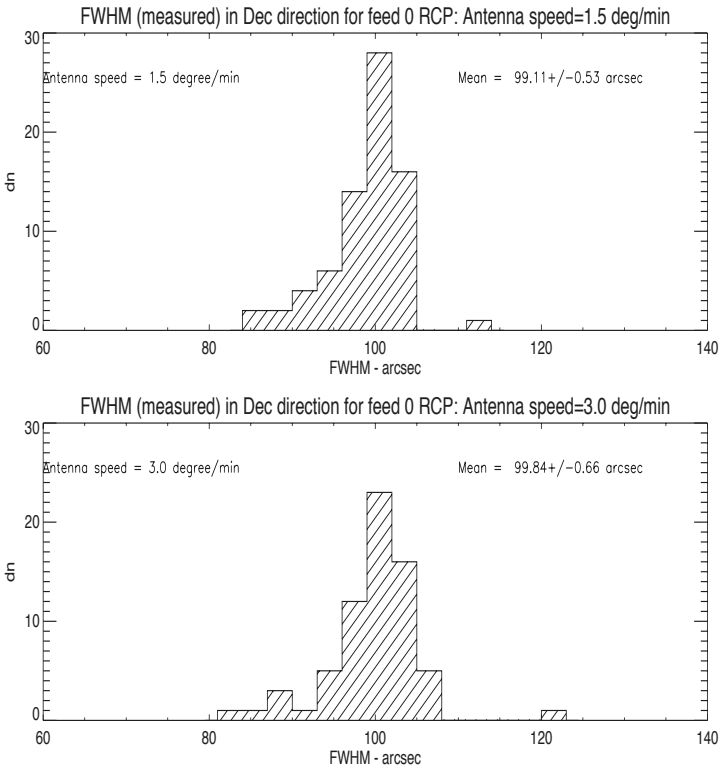

Figure 13: Histogram of the FWHM of the telescope beam (expected $\approx$ 100 arcsec) measured from the Gaussian fit in declination direction for right circular polarization. Top: Scans performed with antenna speed of 1.5°/minute; Bottom: Scans performed with antenna speed of 3.0°/minute

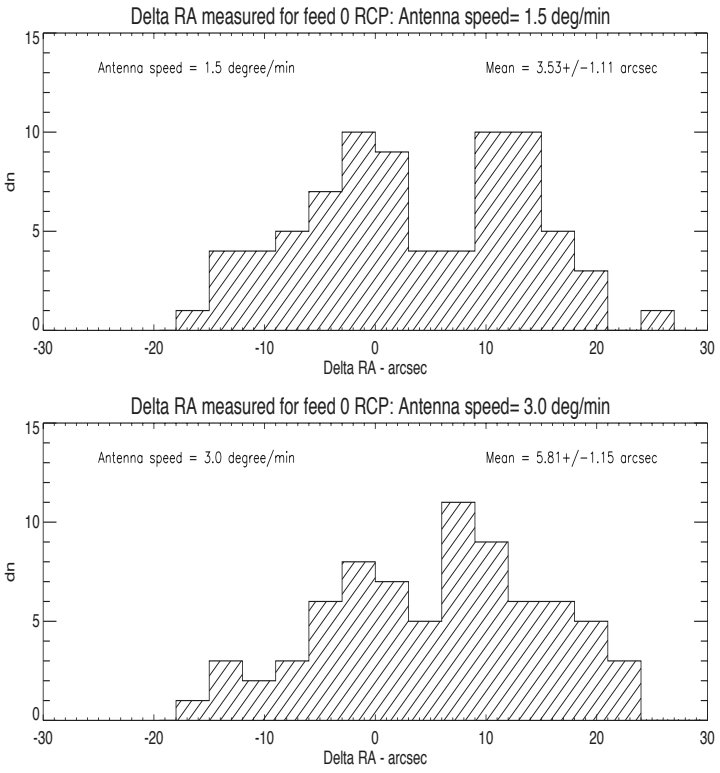

Figure 14: Histogram of the difference between RA taken from the literature and the ones measured from the Gaussian fit in units of arcsec for right circular polarization. Top: Scans performed with antenna speed of 1.5°/minute; Bottom: Scans performed with antenna speed of 3.0°/minute

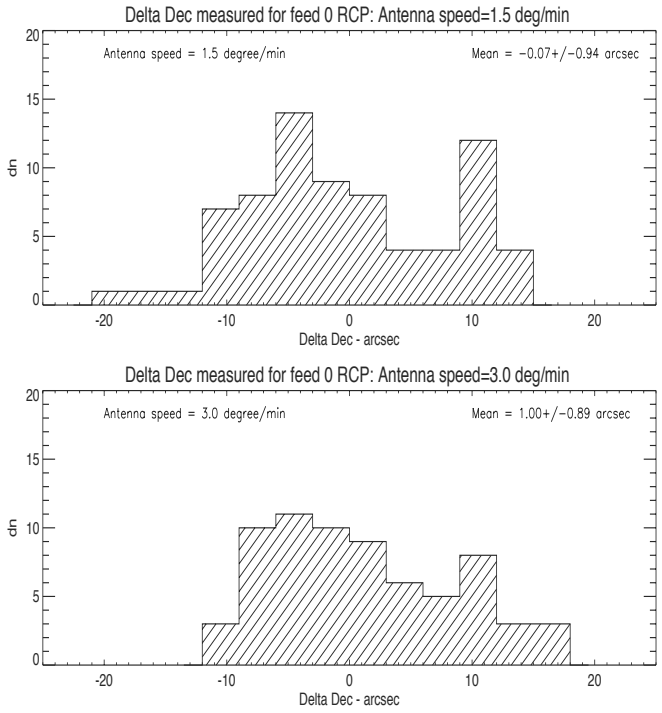

Figure 15: Histogram of the difference between Dec taken from the literature and the ones measured from the Gaussian fit in units of arcsec for right circular polarization. Top: Scans performed with antenna speed of 1.5°/minute; Bottom: Scans performed with antenna speed of 3.0°/minute

Appendix B

In this appendix we show the offsets in RA, Dec and FWHM obtained for sources 3C48 and 3C286. Data are taken from the calibration campaign carried out on 2009, September 27^{th} & 28^{th}.

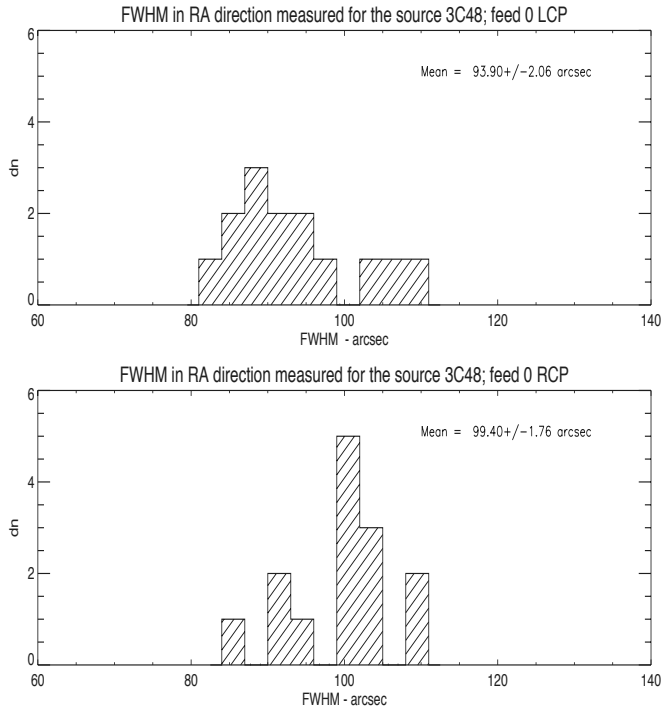

Figure 16: Histogram of the FWHM of the telescope beam (expected $\approx$ 100 arcsec) measured from the Gaussian fit in right ascension direction. Top: Left circular polarization; Bottom: Right circular polarization.

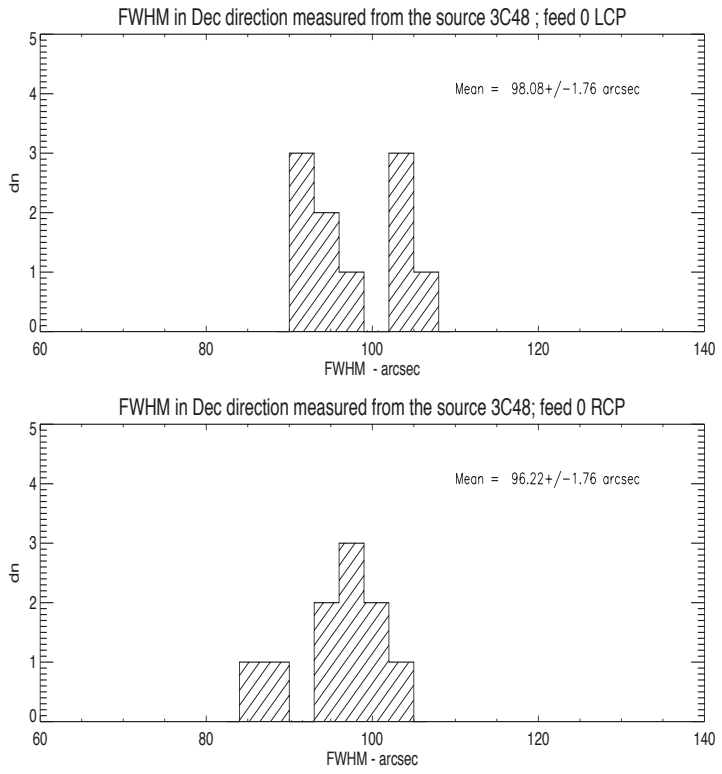

Figure 17: Histogram of the FWHM of the telescope beam (expected $\approx$ 100 arcsec) measured from the Gaussian fit in declination direction. Top: Left circular polarization; Bottom: Right circular polarization.

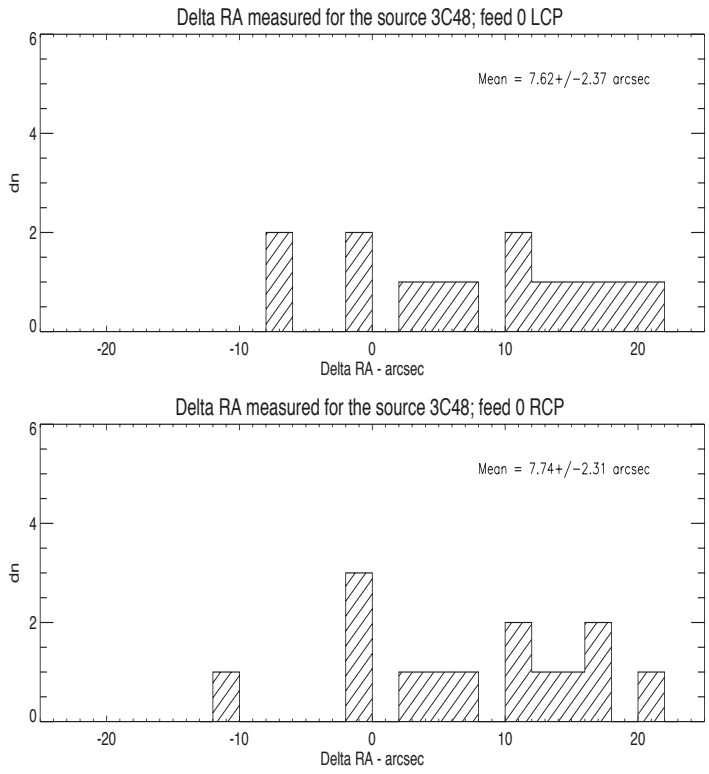

Figure 18: Histogram of the difference between the RA taken from the literature and the ones measured from the Gaussian fit in units of arcsec. Top: Left circular polarization; Bottom: Right circular polarization.

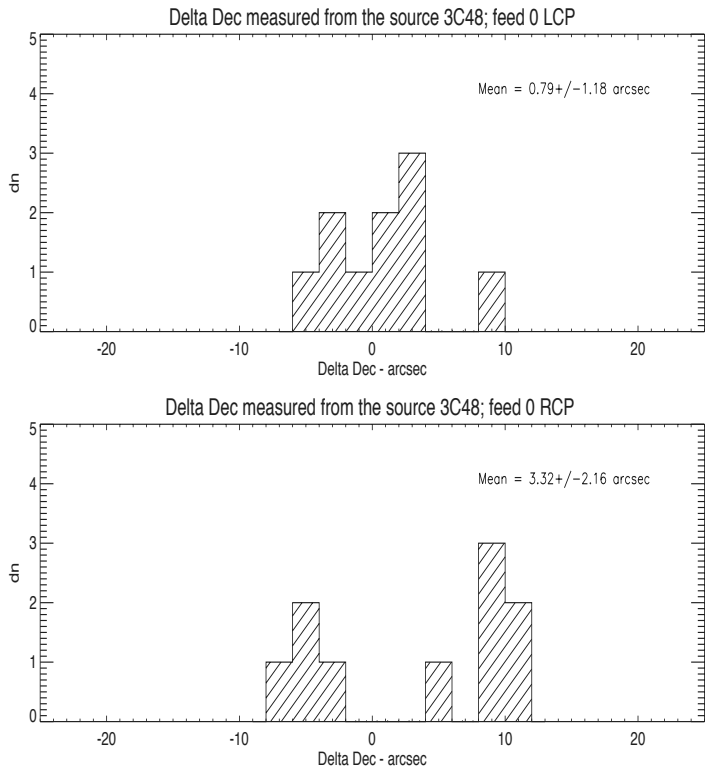

Figure 19: Histogram of the difference between the Dec taken from the literature and the ones measured from the Gaussian fit in units of arcsec. Top: Left circular polarization; Bottom: Right circular polarization.

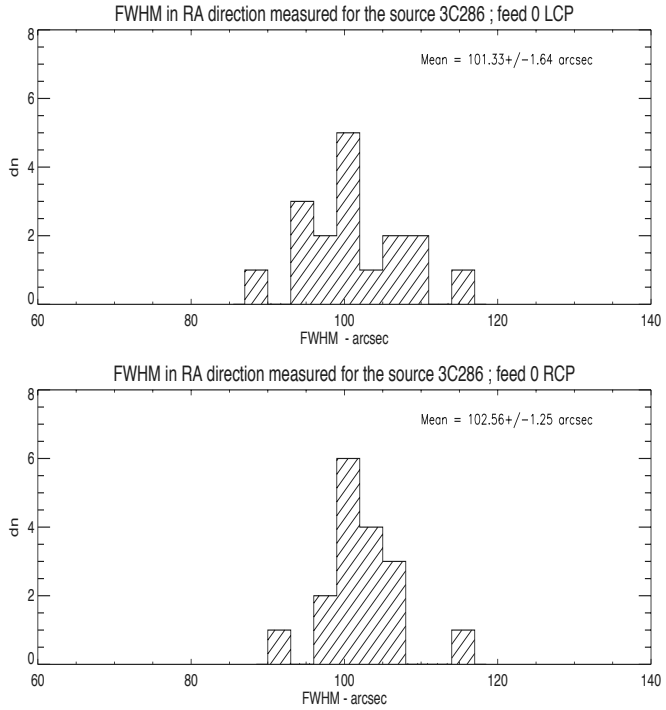

Figure 20: Histogram of the FWHM of the telescope beam (expected $\approx$ 100 arcsec) measured from the Gaussian fit in right ascension direction. Top: Left circular polarization; Bottom: Right circular polarization.

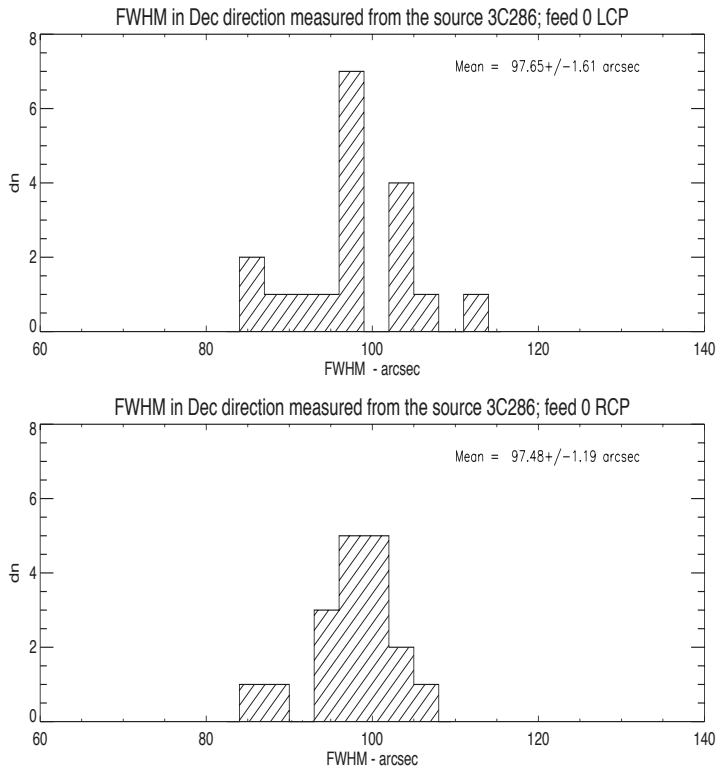

Figure 21: Histogram of the FWHM of the telescope beam (expected $\approx$ 100 arcsec) measured from the Gaussian fit in declination direction. Top: Left circular polarization; Bottom: Right circular polarization.

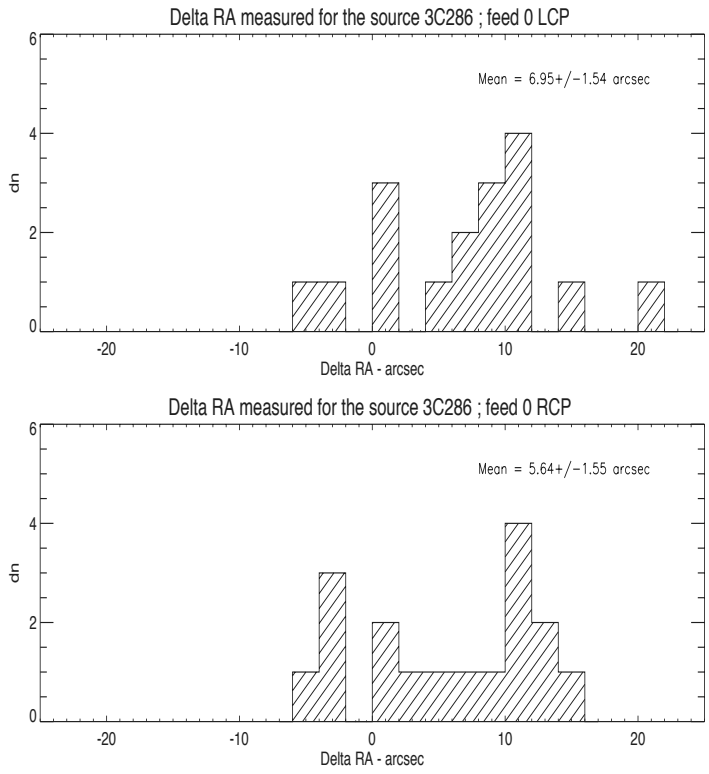

Figure 22: Histogram of the difference between the RA taken from the literature and the ones measured from the Gaussian fit in units of arcsec. Top: Left circular polarization; Bottom: Right circular polarization.

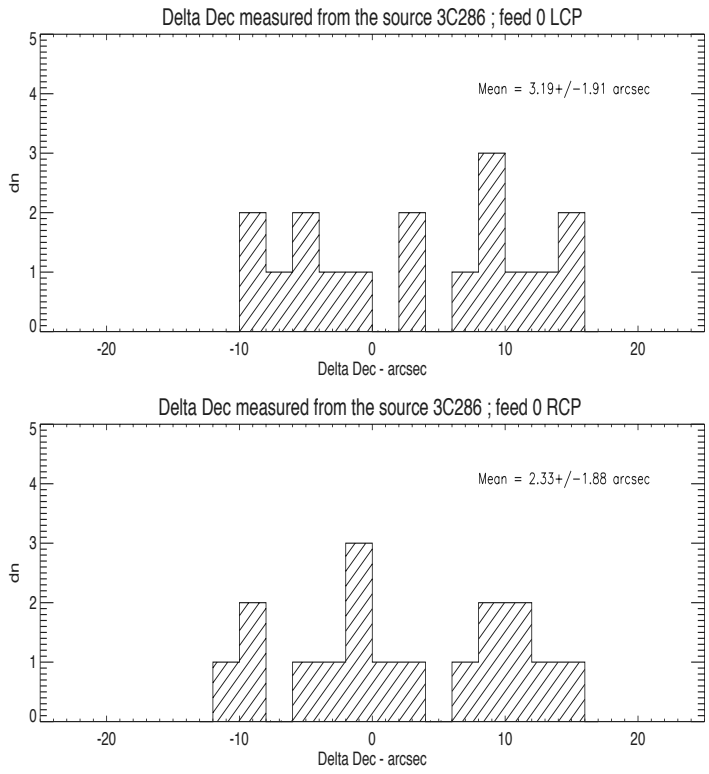

Figure 23: Histogram of the difference between the Dec taken from the literature and the ones measured from the Gaussian fit in units of arcsec. Top: Left circular polarization; Bottom: Right circular polarization.

Appendix C

In this appendix we show the offsets in RA, Dec and FWHM obtained for sources 3C48, 3C286 and 3C147. Data are taken from the pilot survey conducted in winter 2010.

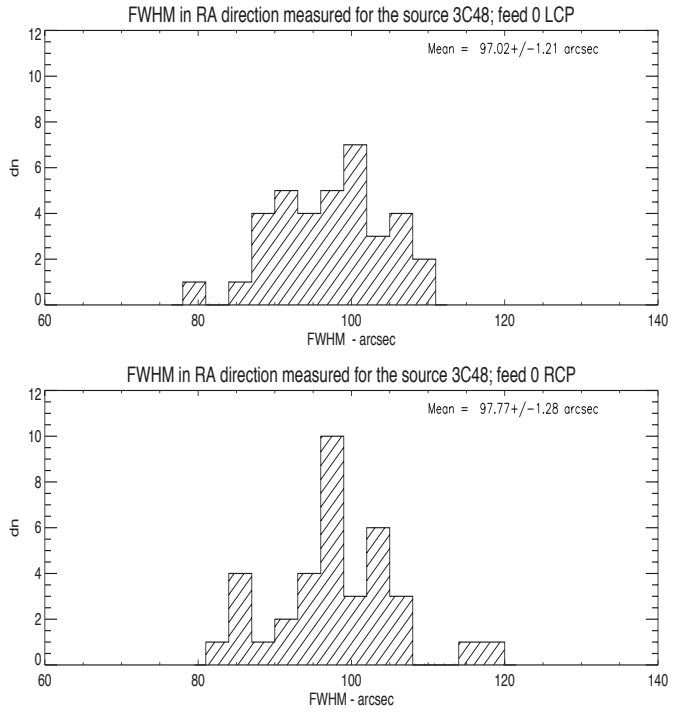

Figure 24: Histogram of the FWHM of the telescope beam (expected $\approx$ 100 arcsec) measured from the Gaussian fit in right ascension direction. Top: Left circular polarization; Bottom: Right circular polarization.

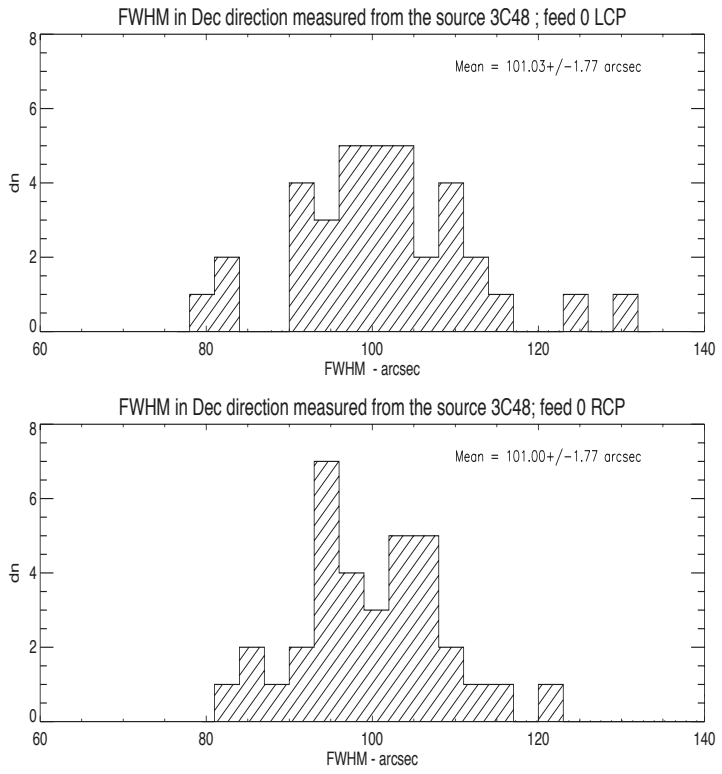

Figure 25: Histogram of the FWHM of the telescope beam (expected ≈ 100 arcsec) measured from the Gaussian fit in declination direction. Top: Left circular polarization; Bottom: Right circular polarization.

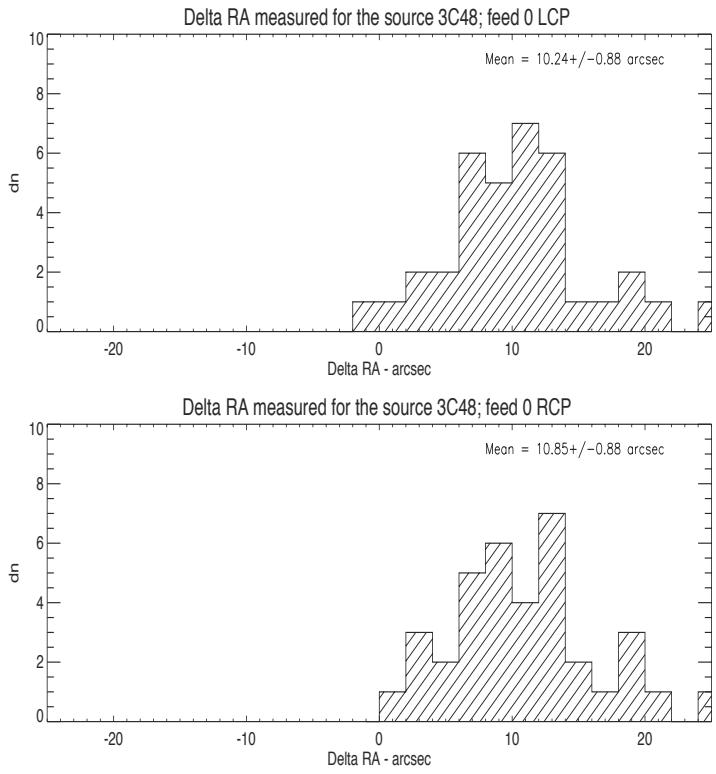

Figure 26: Histogram of the difference between the RA taken from the literature and the ones measured from the Gaussian fit in units of arcsec. Top: Left circular polarization; Bottom: Right circular polarization.

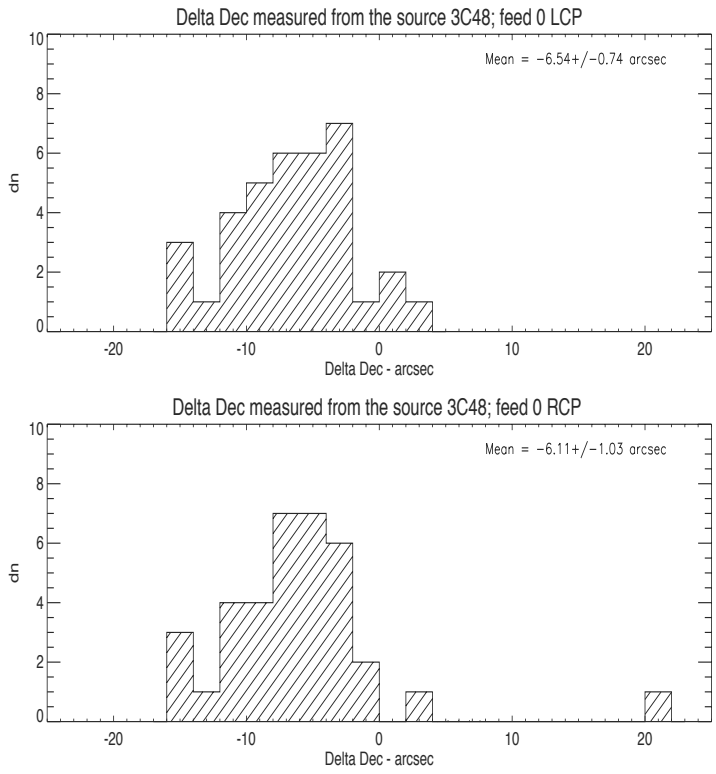

Figure 27: Histogram of the difference between the Dec taken from the literature and the ones measured from the Gaussian fit in units of arcsec. Top: Left circular polarization; Bottom: Right circular polarization.

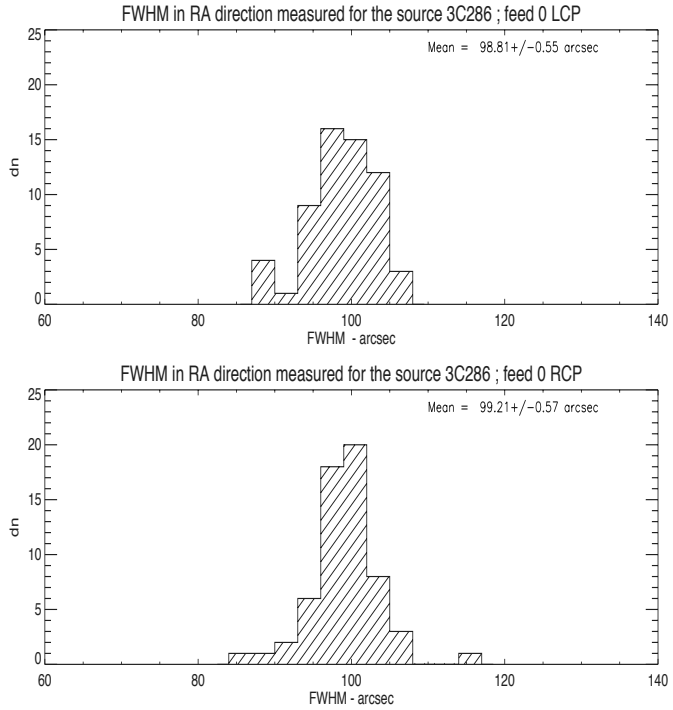

Figure 28: Histogram of the FWHM of the telescope beam (expected $\approx$ 100 arcsec) measured from the Gaussian fit in right ascension direction. Top: Left circular polarization; Bottom: Right circular polarization.

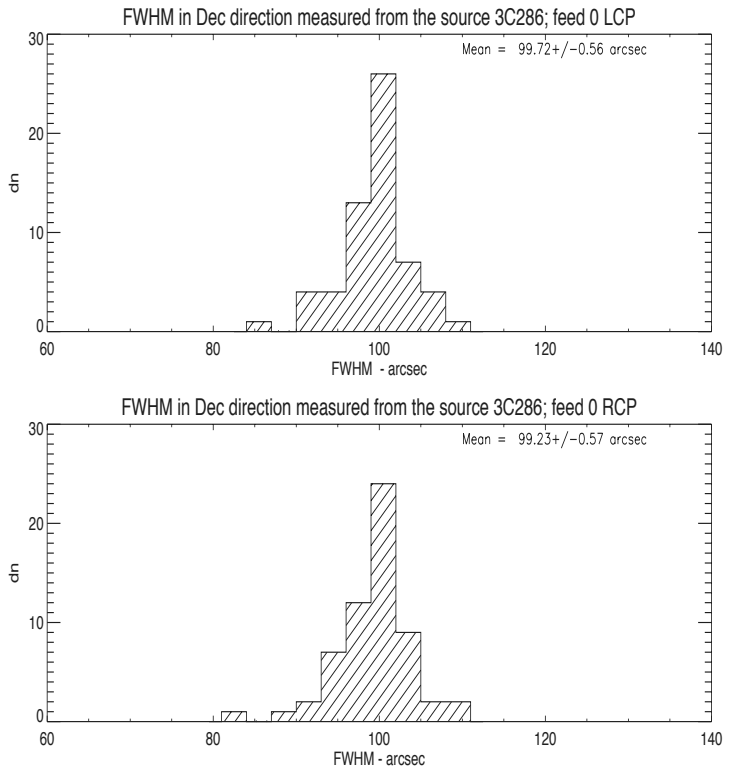

Figure 29: Histogram of the FWHM of the telescope beam (expected $\approx$ 100 arcsec) measured from the Gaussian fit in declination direction. Top: Left circular polarization; Bottom: Right circular polarization.

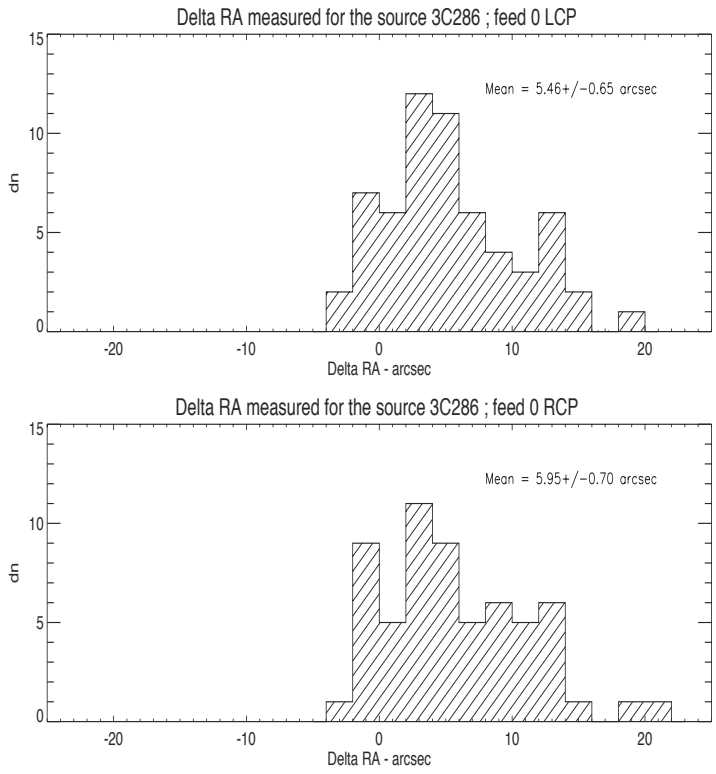

Figure 30: Histogram of the difference between the RA taken from the literature and the ones measured from the Gaussian fit in units of arcsec. Top: Left circular polarization; Bottom: Right circular polarization.

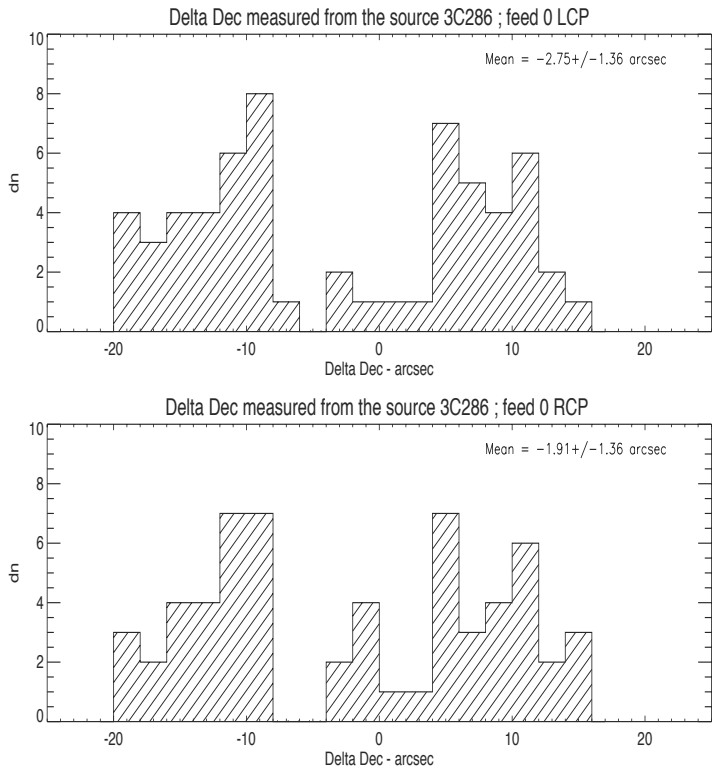

Figure 31: Histogram of the difference between the Dec taken from the literature and the ones measured from the Gaussian fit in units of arcsec. Top: Left circular polarization; Bottom: Right circular polarization.

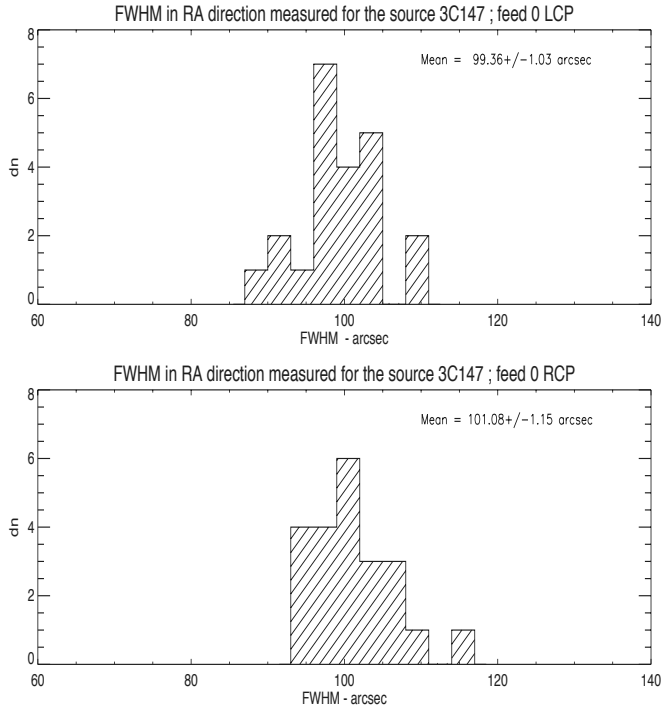

Figure 32: Histogram of the FWHM of the telescope beam (expected $\approx$ 100 arcsec) measured from the Gaussian fit in right ascension direction. Top: Left circular polarization; Bottom: Right circular polarization.

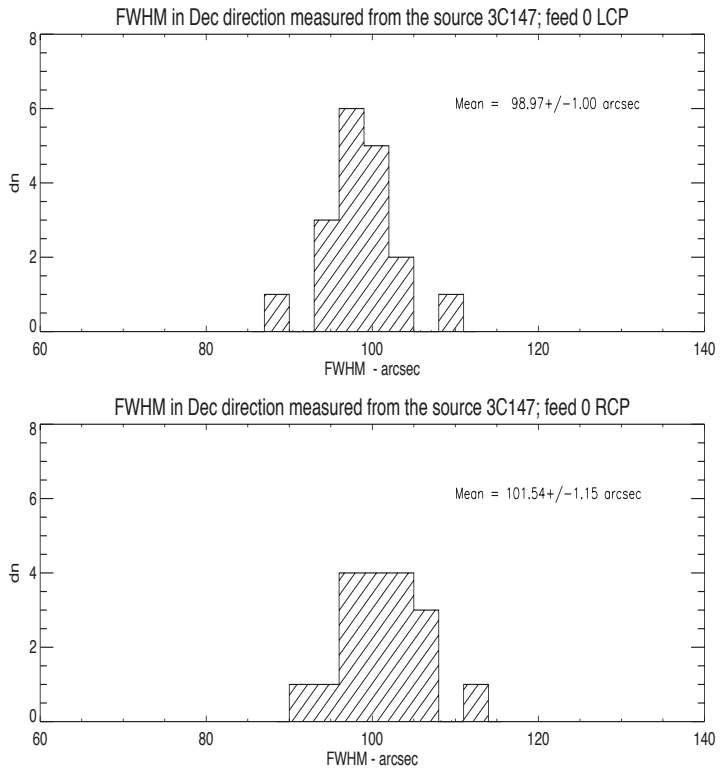

Figure 33: Histogram of the FWHM of the telescope beam (expected $\approx$ 100 arcsec) measured from the Gaussian fit in declination direction. Top: Left circular polarization; Bottom: Right circular polarization.

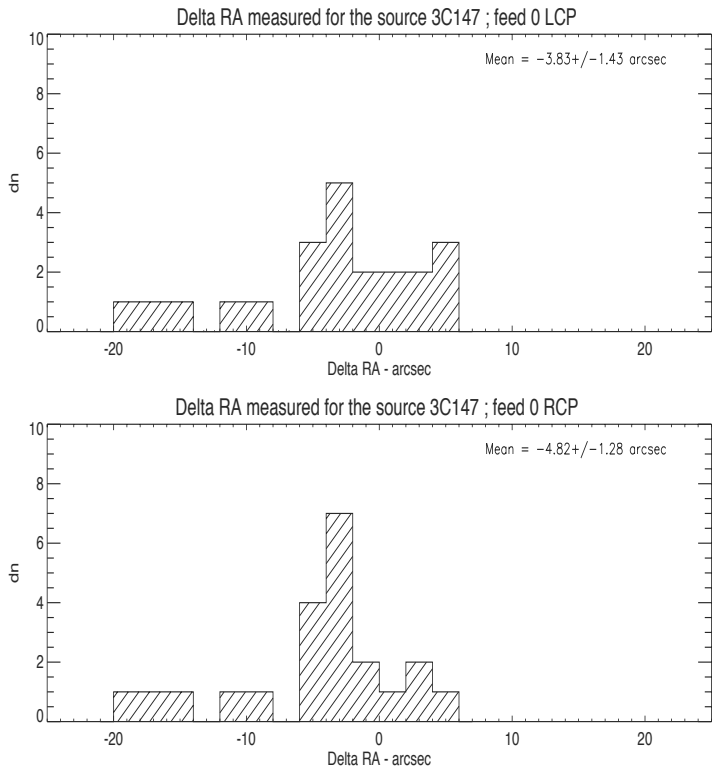

Figure 34: Histogram of the difference between the RA taken from the literature and the ones measured from the Gaussian fit in units of arcsec. Top: Left circular polarization; Bottom: Right circular polarization.

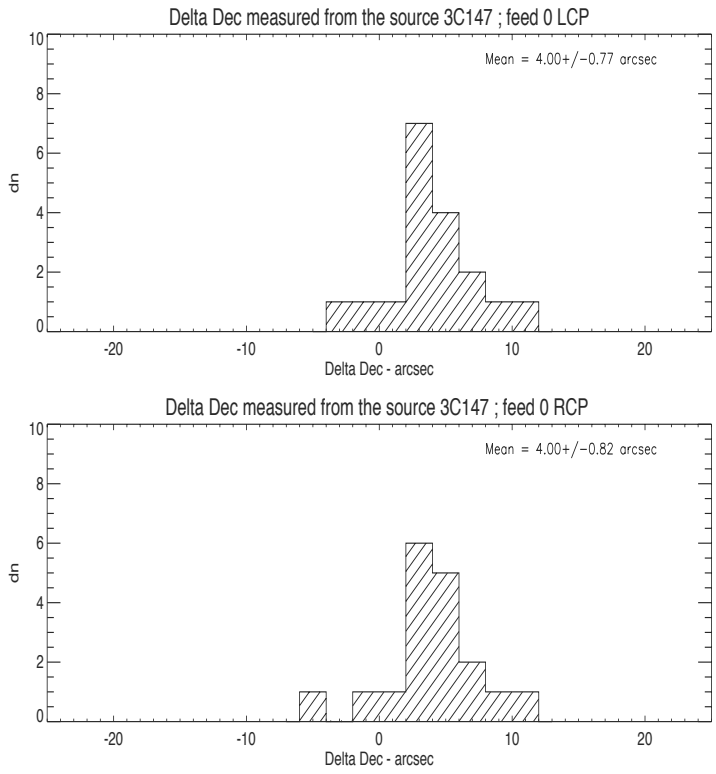

Figure 35: Histogram of the difference between the Dec taken from the literature and the ones measured from the Gaussian fit in units of arcsec. Top: Left circular polarization; Bottom: Right circular polarization.